ACS Sustainable Chemistry & Engineering

Research Article

Cite This: ACS Sustainable Chem. Eng. 2019, 7, 18965−18975

pubs.acs.org/journal/ascecg

Toxicity Evaluation of One-Dimensional Nanoparticles Using *Caenorhabditis elegans*: A Comparative Study of Halloysite Nanotubes and Chitin Nanocrystals

Xiujuan Zhao,[†,∥] Qinli Wan,[‡,∥] Xiaodie Fu,[‡] Xiao Meng,[‡] Xianfeng Ou,[†] Ruowei Zhong,[§] Qinghua Zhou,*[,‡] and Mingxian Liu*[,†]

[†]Department of Materials Science and Engineering, [‡]The First Affiliated Hospital, Biomedical Translational Research Institute, and [§]Internship Program, Biomedical Translational Research Institute, Jinan University, 601 Huangpu Avenue West, Tianhe District, Guangzhou 510632, China

Supporting Information

ABSTRACT: In this study, the toxicity of two one-dimensional (1D) nanoparticles, halloysite nanotubes (HNTs) and chitin whiskers (ChNCs), was investigated in detail. Both in vitro and in vivo models were applied to evaluate the toxicity by cell viability staining, apoptosis assay, and reactive oxygen species generation. Particularly, the toxicity of HNTs and ChNCs was compared using an in vivo model *Caenorhabditis elegans*; their toxicity was assessed using the in vitro models, mouse bone marrow mesenchymal stem cells (mBMSCs) and rat osteosarcoma cells (UMR-106). In vitro, both HNTs and ChNCs exhibited low toxicity at concentrations lower than 50 μg/mL, but HNTs showed higher toxicity than ChNCs at higher concentrations such as 200 μg/mL. Cell viabilities of mBMSCs and UMR-106 were 73.4 and 77.1% at the HNT concentration of 200 μg/mL, while these were 96.2 and 99.8% at the ChNC concentration of 200 μg/mL, respectively. In vivo, HNTs exhibited a side effect on the *C. elegans* reproduction but did not influence the lifespan and other phenotypes, which suggested that HNTs had no long-term toxicity effects. While ChNCs did not result in obvious alterations in the phenotype of worms below the concentration of 2.5 mg/mL, the brood size of *C. elegans* decreased at ChNC concentrations of 10 and 50 mg/mL. Moreover, ChNCs had the side effect on the development of *C. elegans* at the high level. However, ChNC exposure at the concentrations of 10 and 50 mg/mL induced the longer fast movement periods and extended lifespan of *C. elegans*. It demonstrated that both HNTs and ChNCs had good biocompatibility below the concentration of 2.5 mg/mL. The toxicity studies of these two 1D nanoparticles contributed to their great significance for various biomedical applications.

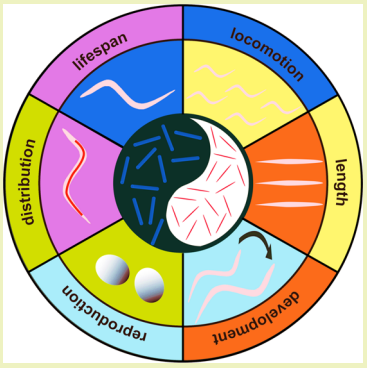

KEYWORDS: *Caenorhabditis elegans, halloysite nanotubes, chitin whisker, nanotoxicity*

INTRODUCTION

Nanotoxicity study becomes more and more significant with emphasis on the unpredictable biosafety during the explosive growth of synthetic and natural nanomaterials.[1,2] One-dimensional (1D) nanoparticles, such as nanotubes, nanowires, nanofibers, nanobelts, and nanorods, have attracted the researchers' interests from the unique structures such as a high aspect ratio and anisotropy, which leads to the excellent mechanical, electrical, and magnetic properties of particles.[3] Recently, researchers have found that the shape of 1D nanoparticles played the important role in the cell uptake kinetics and toxic mechanism.[4] Kostarelos et al. found that the cellular uptake of functionalized carbon nanotubes (CNTs) is independent of the functional group and cell type. Mammalian and prokaryotic cells can uptake CNTs through the different cellular barriers by energy-independent mechanisms. The cylindrical shape and high aspect ratio of CNTs ensure a "nanosyringe" uptake mechanism for their penetration through the plasma membrane. The size and shape of gold nanoparticles can mediate receptor−ligand binding constants, receptor recycling rates, and exocytosis. The rod-shaped nanoparticles can have larger contact area with the cell membrane receptors than the spherical nanoparticles when the longitudinal axis of the rods interacts with the receptors.[5] However, the toxicity of other type 1D nanoparticles such as clay and polysaccharide nanocrystals has rarely been investigated.

Halloysite nanotubes (HNTs), $Al_2Si_2O_5(OH)_4{\cdot}nH_2O$,[6] have a tubular-like shape with a high aspect ratio of 10−50 (L/D). The length and the outer diameter of HNTs range from 200 to 2000 nm and from 40 to 70 nm, respectively.[7,8] The inner and outer surfaces of HNTs are composed of Al_2O_3 and SiO_2, which are positively and negatively charged, respectively.[9] However, the overall potential of HNTs is negative. The hollow tubular structure enables them with excellent properties such as carrying and sustained release of active agents,

Received: July 28, 2019
Revised: September 24, 2019
Published: November 4, 2019

DOI: 10.1021/acssuschemeng.9b04365
ACS Sustainable Chem. Eng. 2019, 7, 18965−18975

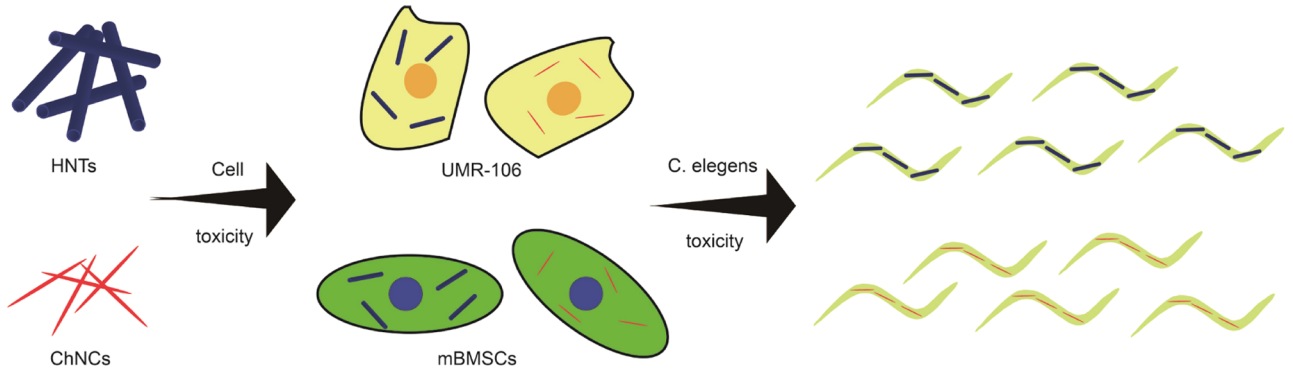

Figure 1. Toxicological evaluation of HNTs and ChNCs.

mechanical reinforcement, thermal stability, or the other transport properties.[8,10,11] Owing to the excellent biocompatibility of HNTs, they have been applied in tissue engineering scaffold, wound healing dressing, drug delivery, and biosensors.[12−14] Massaro et al. reviewed the biomedical applications of HNTs.[15] HNTs could be modified by carbon dots (CDs) to develop fluorescent tags.[16] HNT-CDs could load and release calf thymus-DNA as the nonviral vector for oral gene therapy with the tubular body protecting and provide sustained release of drugs. In addition, HNT-CDs also had the ability of tracking the delivered molecules.[17]

With the widespread applications of HNTs, it is very essential to investigate the toxicity of HNTs. The *Caenorhabditis elegans*, zebrafish, and mice models have been used to evaluate the toxicity of HNTs.[18−20] The interaction between cells or tissue and HNTs is a critical issue that will determine any future biological application of such structures. Laser confocal visualization and atomic force microscopy (AFM) of cellular uptake exhibited that fluorescently labeled HNTs are located within the cells in the nuclear vicinity.[21,22] Fakhrullina et al. used enhanced dark-field microscopy to investigate the in vivo toxicity of HNTs using *C. elegans*. It was found that HNTs is localized exclusively in the alimentary system and does not induce severe toxic effects on nematodes.[18] Recently, the toxic effects of HNT-supported palladium nanoparticles on the plants were explored. The results showed HNT-supported palladium nanoparticles had no influence on radish seed germination physiology, seedling development and growth, mitotic index, and chromosomal figures.[23]

Chitin is a natural polysaccharide extracted from the skeletal of crustaceans, insects, and algae.[24] With good biocompatibility, biodegradability, and antibacterial activity, chitin and its derivatives have been extensively used in food, medicine, cosmetic, and environmental industries over the past decades.[25] Chitin whiskers (ChNCs), the acidolysis product of chitin, exhibit a rodlike shape and maintain the bioactivity of chitin, and their advantages include a high modulus, large specific surface area, and high aspect ratio, which facilitate their application as biomedical materials and nanoreinforcement of polymers.[26−29] In contrast to negatively charged HNTs, the ζ potential of ChNC suspension is positive because the presence of NH_2 on the surface of ChNC molecules.[30] However, as elongated rodlike particles, biological safety of ChNCs is worth exploring in light of that nanomaterials may interact with living systems, causing a threat to human health.[31] One of the biomedical applications of these polysaccharide nanocrystals is as a nanovector for therapeutic agent delivery. For example, ChNCs were explored as carriers of methylparaben to prepare durable antimicrobial cotton textiles.[32] Our laboratories have also investigated the use of ChNC scaffolds in controlling the release of curcumin for anticancer therapy.[33] However, studies on the toxicity of ChNCs especially using an in vivo model are very rare.

Over the past decades, it has been proved that *C. elegans* can be used as an animal model for studies on toxicity.[34,35] Considering these advantages including a short life cycle, a small size, good transparency, and a fully sequenced genome, *C. elegans* was often chosen as the priority model to elucidate the toxicity mechanism.[18,36−38] Previous studies demonstrated that *C. elegans* could swallow the nanoparticles as their baits.[39−42] The nanoparticles were used as a food source for *C. elegans*, which is the simple and convenient way to study the toxicity.[16] In the present work, the physical−chemical features of the two 1D nanoparticles have been investigated. Then, mouse bone marrow mesenchymal stem cells (mBMSCs) and rat osteosarcoma cells (UMR-106) were used to evaluate the in vitro cytotoxicity of the nanoparticles. In addition, the in vivo toxicities of HNTs and ChNCs at concentrations from 0 to 50 mg/mL using *C. elegans* were assessed and compared. It demonstrated that both HNTs and ChNCs had good biocompatibility at low concentrations. The toxicity studies of these two 1D nanoparticles contributed to their great significance for various applications.

EXPERIMENTAL SECTION

Materials. HNTs were purchased from Guangzhou Runwo Materials Technology Co., Ltd. HNTs were purified by a dispersion−centrifugation method. Raw halloysite suspensions with a concentration of 2% (w/v) were prepared. After keeping the suspension for 24 h, the upper solution was centrifuged at 8000 rpm and then freeze-dried. After repeating the standing and freeze-drying three times, the purified halloysite was obtained with a purity higher than 95.7 wt %. ChNCs were prepared by the acid hydrolysis of crab shells (Wuhan Hezhong Biochemical Manufacturing Co., Ltd., China), according to a previous study.[43] Rhodamine-labeled HNTs and ChNCs were prepared by absorbing rhodamine B (Aladdin).[19] In detail, 1 g of HNTs or ChNCs and 5 mg of rhodamine B were added into 50 mL of deionized (DI) water and were stirred for 24 h away from light. Then, the suspensions were centrifuged at 8000 rpm for 3 min. To separate the free rhodamine B, 100 mL of deionized water was added into the centrifugal deposit and mixed evenly. Free rhodamine B could be soluble in water and removed by centrifugation. The washing process was repeated three times. Rhodamine-labeled HNTs and ChNCs could be obtained after freeze-drying. Acridine orange (AO) and ethidium bromide (EB) were bought from Solarbio Science & Technology Co., Ltd., China. Cell Counting Kit-8 (CCK-8) reagents were bought from BestBio Biology Co., Ltd., China. Ultrapure DI water was obtained by

DOI: 10.1021/acssuschemeng.9b04365
ACS Sustainable Chem. Eng. 2019, 7, 18965−18975

deionization and filtration with a Millipore purification apparatus (resistivity >18.2 MΩ cm).

Material Characterization. The morphologies of HNTs and ChNCs were observed by scanning electron microscopy (SEM, Ultra 55, Zeiss, Germany), transmission electron microscopy (TEM, JEM-2100F, JEOL Ltd., Japan), and atomic force microscopy (AFM, BioScope Catalyst Nanoscope-V, Bruker Instruments Ltd.) with a sample concentration of 0.5 mg/mL. The morphologies of nanoparticles were imaged by ScanAsyst mode with the probes (Tap 150 AI-G). The particle size distribution and ζ potential of the nanoparticles were analyzed using a Zetasizer Nano ZS instrument (Malvern Instruments Ltd., U.K.) with a sample concentration of 0.35 mg/mL.

Cell Culture. To investigate the toxicities of the nanoparticles systematically, toxic evaluations of cells and *C. elegans* were performed (Figure 1). Mouse bone marrow mesenchymal stem cells (mBMSCs) and rat osteosarcoma cells (UMR-106) were purchased from American Type Culture Collection (Manassas, VA) and were used to evaluate the toxicity in vitro. The cells were cultured in high glucose-Dulbecco's modified Eagle's medium supplemented with 10% (v/v) fetal bovine serum and 1% (v/v) penicillin−streptomycin solution. All cells were maintained in a 37 °C incubator with a humidified atmosphere of 5% CO_2.

Cytotoxicity and LIVE/DEAD Staining Assays. mBMSCs and UMR-106 were seeded in 96-well culture plates with the concentrations of 1×10^4 and 5×10^3 cells/well for 24 h, respectively. In this study, nanoparticle suspensions of different concentrations (25, 100, 500, and 2000 μg/mL) were prepared and sterilized using a microwave with 400 W power for 1 min. Then, sterilized nanoparticle suspensions were added into the culture plates with the final concentration (2.5, 10, 50, and 200 μg/mL) to incubate for 24 h. The cell cultures were not contaminated. The CCK-8 assay was used to evaluate the cytotoxicity of 1D nanoparticles, and AO/EB dual-fluorescent dyes were used to observe dead and living cells.

Confocal Laser Scanning Microscope (CLSM) Observation. mBMSCs were cultured for 24 h with the rhodamine-labeled nanoparticles and then fixed by paraformaldehyde. Cell membranes were penetrated using Triton, and the cells were stained by the corresponding markers. Finally, rhodamine-labeled nanoparticles, cytoskeletons, and nuclei stained by Alexa Fluor 488 phalloidin and 4′,6-diamidino-2-phenylindole, respectively, were observed by the CLSM (Leica, SP8, Germany).

Cell Apoptosis Assay and Reactive Oxygen Species (ROS) Assay. The flow cytometry assay was used to determine the cell apoptosis and ROS. mBMSCs were seeded into six-well plates (5×10^5 cells per well) for 24 h. Different concentration nanoparticles were added in the culture plates, and cells were collected after incubating for 24 h. An annexin V−fluorescein isothiocyanate (FITC)/propidium iodide (PI) apoptosis detection kit (eBioscience) and the dichlorodihydrofluorescein diacetate assay were used to measure the cell apoptosis and ROS production, respectively.

Maintenance of *C. elegans* and Treatment. Wild-type N2 *C. elegans*, obtained from Caenorhabditis Genetic Center (University of Minnesota), which is supported by the NIH NCRR, were used in this study. The maintenance of worms was conducted as previously described, unless otherwise stated.[44] Synchronization of worms was performed by preparing eggs from gravid adults using a solution (containing 7 mL of ddH_2O, 1 mL of 5 M NaOH, and 2 mL of 6−12% NaOCl); eggs were washed twice with M9 buffer and hatched overnight in M9 buffer to synchronize to L1 larvae; then, L1 larvae were raised on nematode growth medium (NGM) agar plates seeded with *Escherichia coli* OP50 at 20 °C according to standard methods for the following experiment. The nanoparticle dispersion was sonicated (30 min) prior to use for exposure. Nematode growth media (NGM) plates containing compounds were equilibrated overnight before use.

Distribution and Translocation. Worms were exposed to raw nanoparticles and rhodamine-labeled nanoparticles from L1 larvae for 24 or 48 h, then washed three times with M9 buffer, and imaged using a Nikon Ti2-U microscope.

Lifespan Assay. All strains were grown on nematode growth medium (NGM) agar plates seeded with *E. coli* OP50 at 20 °C according to standard methods for two to three generations without starvation. All lifespan assays were performed at 20 °C as previously described.[44−46] In brief, about 100 late L4 larvae or young adults were transferred to fresh plates containing the respective nanoparticles and 10 μM 5-fluro-2′-deoxyuridine (Sigma) and scored every day. To ensure fresh food, worms were transferred using worm pick every second day. Animals were denoted dead if they failed to display mechanical stimulation-induced movement with a pick. Sixty worms were examined per experiment.

Movement Assays. Movement assays were conducted as previously described.[32] Briefly, about 100 late L4 larvae or young adults were transferred to fresh plates with or without 1D nanoparticles as described in the lifespan assay. When tapping plates, the movement of worms in a continuous, coordinated sinusoidal way was defined as fast movement; otherwise, the movement of worms was characterized as a nonfast movement.

Fertility Assay. Single L4 or young adults were transferred to single plates with or without 1D nanoparticles and then transferred every 24 h to a fresh plate. The number of eggs and hatched larvae were determined by each worm on each day. The hatching rate was calculated as the number of larvae/number of egg. For each exposure, more than 30 worms were used and the experiments were conducted three times.

Development Analysis. The effects of different concentrations of HNTs and ChNCs on the development of worms were determined by calculating the percentage of L4 worms in the worm population. The embryos that had been laid within an interval of 4−6 h were maintained on the plates with or without the nanoparticles, after 48 h, by counting the number of L4 worms.

ROS Production. The worms that were raised on the plates with or without HNTs and ChNCs were labeled using MitoSOX as previously described.[47,48] Labeled animals were picked on the agar pads and then imaged at 20× magnification using a Nikon Ti2-U fluorescence microscope. At least, 30 animals were used for each experiment and each experiment was repeated at least twice. For fluorescence quantification, images were analyzed by ImageJ.

Oil Red O (ORO) Staining and Quantification. ORO staining of fixed worms was conducted as previously described.[49] ORO-stained worms were picked onto agar pads and imaged at 20× magnification using a Nikon Ti2-U fluorescence microscope. The ORO intensity was measured using Image-Pro-Plus processing software. At least 30 animals were used for each experiment, and each experiment was repeated at least twice.

Quantitative Reverse Transcription Polymerase Chain Reaction (PCR) Assay. RNAiso Plus (Takara) was used to isolate total RNA of worms based on the protocol. The synthesis of complementary DNA (cDNA) using total RNA through a high capacity cDNA transcription kit (Applied Biosystems) based on the manufacturers' protocol. Expression levels of examined genes were analyzed in a SYBR Green Select Master Mix (Applied Biosystems) on a CFX96 real-time system (Bio-Rad). Triplicate reactions were conducted. The results were calculated by the $2^{-\Delta\Delta Ct}$ method and normalized to the reference genes cdc-42.[50] The following quantitative PCR (qPCR) primer sequences were used:

sod-3: 5′ AGCATCATGCCACCTACGTGA and 5′ CACCAC-CATTGAATTTCAGCG;

ctl-1: 5′ AGACGTATCCAAAACCCCAAGT and 5′ GACCGTT-GAAAAACGAACGAGAA;

dod-3: 5′ CGTATATGGACCCAGCTAATG and 5′ ATGAA-CACCGGCTCATTC.

Intestinal Barrier Function Assay. The intestinal barrier function assay was performed as previously described.[51] Briefly, the worms were raised on the plates with or without HNTs and ChNCs until young adult stage. Then, animals were collected using M9 buffer and suspended for 3 h in liquid medium containing *E. coli* OP50 and blue food dye (Spectrum FD&C Blue #1 PD110, 5.0% w/v in water). Then, blue food dye-stained worms were picked onto agar pads and imaged at 20×/40× magnification using a Zeiss Axio Imager Z2 with

DOI: 10.1021/acssuschemeng.9b04365
ACS Sustainable Chem. Eng. 2019, 7, 18965−18975

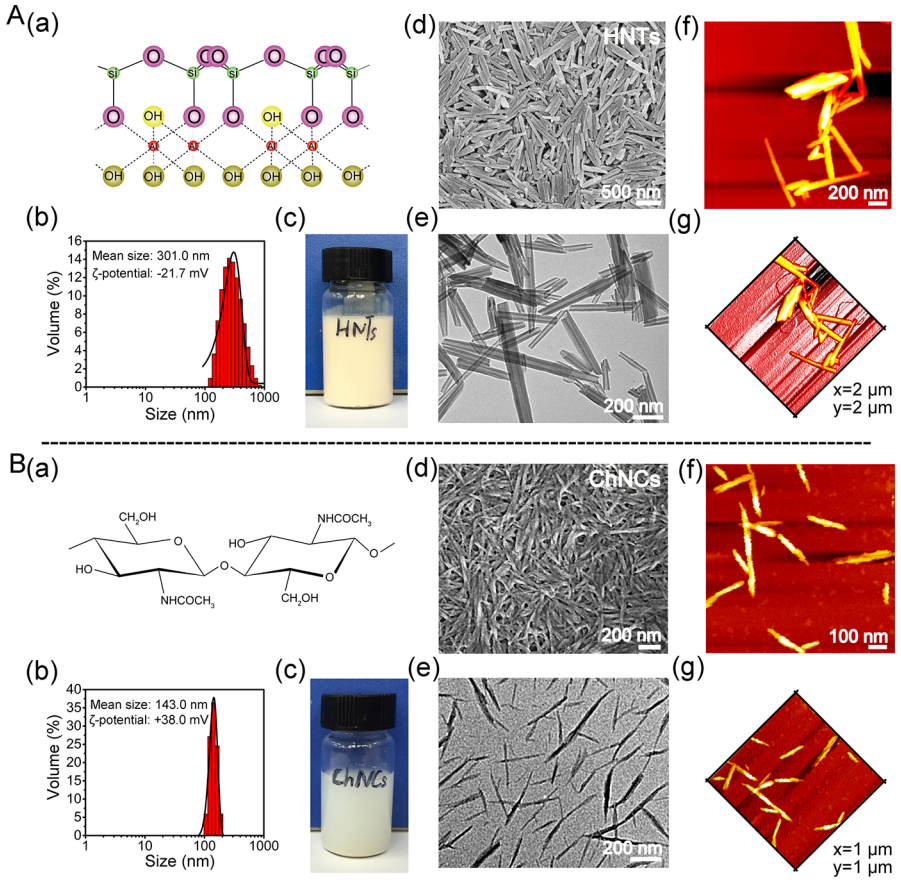

Figure 2. Characterization of HNTs and ChNCs. (A-a, B-a) Molecular formula; (A-b, B-b) size distribution and ζ potential; (A-c, B-c) appearance of the aqueous dispersion of the two nanoparticles; (A-d, B-d) SEM images; (A-e, B-e) TEM images; (A-f, B-f) AFM images; and (A-g, B-g) AFM 3D images.

ApoTome.2 microscope. For each experiment, at least 30 animals were used and each experiment was repeated at least twice.

Data Analysis. In the statistic experiments, the samples were conducted at least in triplicate and the results were presented as mean ± standard deviation (SD). The results were analyzed using Student's *t* test. $p < 0.05$ represented that it was significant statistically. For the lifespan assay, statistical analysis and mean lifespan were obtained by SPSS software and *p* values were calculated by a log-rank test.

RESULTS AND DISCUSSION

Characterization of HNTs and ChNCs. The chemical composition, morphology, and size characterization result of HNTs and ChNCs are shown in Figure 2. From the structural formulas of HNTs and ChNCs, both of them have massive hydroxyl groups that lead to the good hydrophilicity. HNTs are inorganic matter composed of silicon oxide and aluminum oxide, while ChNCs are organic matter composed mainly of carbon, oxygen, and nitrogen. It indicates that it is feasible to absorb the rhodamine B dye because they are polar and hydrophilic. Figure 2A-c,B-c shows that HNT and ChNC dispersions with the concentration of 8% (w/v) could be stable after ultrasonic dispersion for a long time due to charge repulsion. It could be seen that the nanoparticle suspension could retain good stability after standing for 3 days (Figure S1). Both of them displayed a uniform nanoscale dispersion state, which is beneficial for the uptake by cells and animals. It is determined that the HNTs exhibited negative charges with a ζ potential of −21.7 mV, while ChNCs showed positively charged surfaces with a ζ potential of +38.0 mV. TEM, SEM, and AFM of HNTs and ChNCs demonstrated their rod-like morphology with a high aspect ratio. The length of HNTs ranged from 200 to 1000 nm, and TEM images showed that their empty lumen structure with inner and outer diameters of 10−15 and 50−70 nm, respectively. Lengths and widths of ChNCs were 100−500 and 15−30 nm, respectively. Figure 2A-b,B-b gives the average size of HNTs and ChNCs, i.e., 301 and 143 nm, which indicated that ChNCs had the smaller particle size than HNTs. Since nanoparticles with the high surface reactivity could penetrate the cell membrane and be uptake by cells. The nanoparticle size had an important effect on the toxicity. Recent studies showed that nanoparticles with the particle size <100 nm always had more toxicity than the nanoparticles with large sizes (>100 nm).[52,53]

Cytotoxicity of HNTs and ChNCs in Vitro. In this study, mBMSCs and UMR-106 were selected as the cell model to evaluate the cytotoxicity. At present, a lot of cell lines were applied for studying the toxic effects of nanoparticles.[54−56] Stem cells had a pluripotent nature and self-renewal property. Some findings suggested that primary cells or stem cells responded differently to nanoparticle exposure as compared to the other cell lines.[57,58] The unique properties ensure stem cells to possess the potential applications include stem cell therapy, tissue engineering, drug delivery, and so on. Therefore, evaluating the hazardous effects of 1D nanoparticles on stem cells is significant.[58,59] In our previous studies, it was proved that ChNCs and HNTs could be used as the carrier of antitumor drugs.[33,60] Based on these applications, UMR-106

DOI: 10.1021/acssuschemeng.9b04365
ACS Sustainable Chem. Eng. 2019, 7, 18965−18975

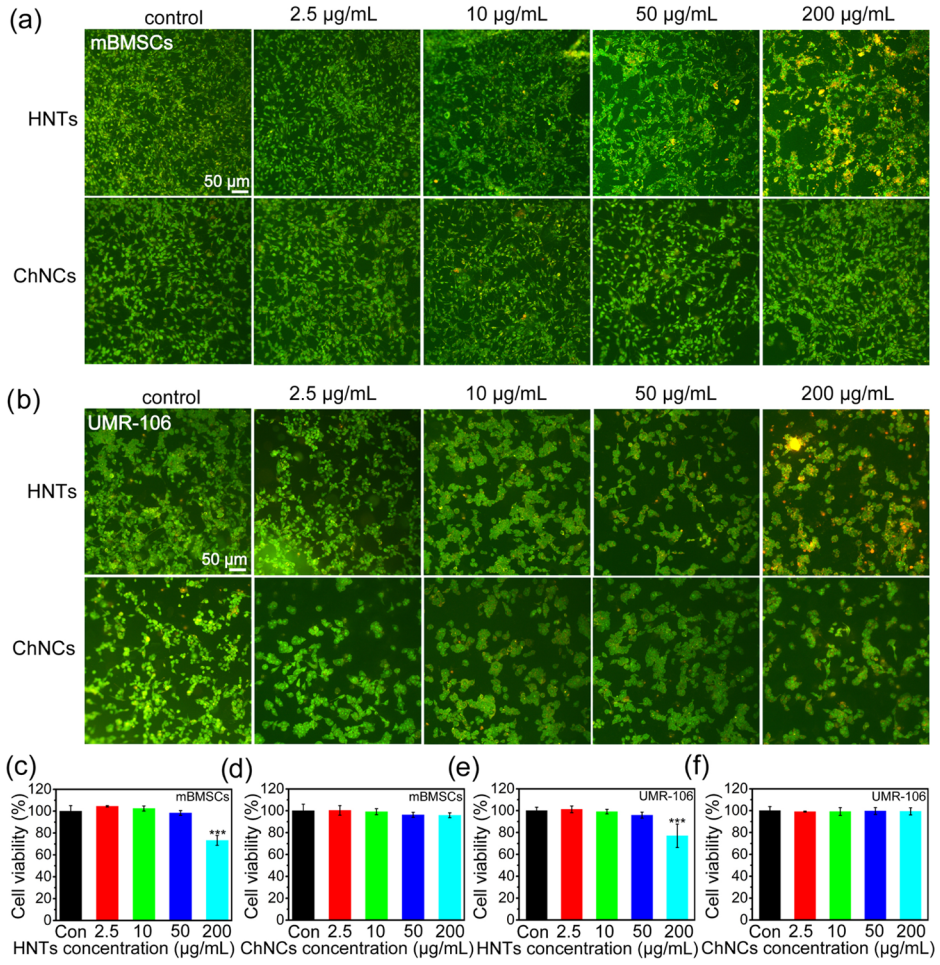

Figure 3. Cytotoxicity of HNTs and ChNCs in vitro. LIVE/DEAD staining images of mBMSCs (a) and UMR-106 (b) cultured for 24 h. Relative survival rate of mBMSCs cultured with HNTs (c) and ChNCs (d) and UMR-106 cultured with HNTs (e) and ChNCs (f) for 24 h (means ± SD, n = 4).

was chosen as the tumor cell model for the cytotoxicity test. As shown in Figure 3, both mBMSCs and UMR-106 were alive and dead cells (orange color) were rare at the concentration of ChNCs in the range of 2.5−200 μg/mL from the LIVE/DEAD staining images. Both HNTs and ChNCs groups did not show obvious difference of LIVE/DEAD staining images at the concentration below 50 μg/mL. However, the HNT group showed more dead cells including mBMSCs and UMR-106 at the concentration of 200 μg/mL. This is properly because the high concentration of nanotubes affects the transportation of the nutrients for cell growth. Results of cell viability also were agreed with it from the CCK-8 measurement. Both HNTs and ChNCs exhibited low toxicity at a concentration lower than 50 μg/mL with the higher cell viabilities of 95%. Cell viabilities of mBMSCs and UMR-106 were 73.4 and 77.1% at the HNT concentration of 200 μg/mL. Cell viabilities of mBMSCs and UMR-106 were 96.2 and 99.8% at the ChNC concentration of 200 μg/mL. It was indicated that both ChCNs and HNTs have low toxicity below 50 μg/mL concentration and ChNCs showed better cytocompatibility at the 200 μg/mL concentration. The toxicity mechanism of HNTs is related to their aluminum elements in the chemical composition.[20] The external surfaces of HNTs were composed of SiO_2, which was first exposed into the cellular media. Asbestos was also a silicate mineral with the fibrous structure. Compared with HNTs, asbestos had the longer fibrous structure (5−20 μm length) and showed the higher in vivo toxicity. However, HNTs with a shorter size (200−1000 nm) could be much easier removal by macrophages.[21] Therefore, HNTs exhibited low toxicity below 50 μg/mL concentration, which can be attributed to the shorter length, while the ChNCs at 200 μg/mL concentration had the better cytocompatibility. ChNCs were composed of the pyranose rings that had the good biocompatibility and nontoxicity.[61] It results in the better cytocompatibility of ChNCs because of the chemical composition of nanoparticles.

To confirm the uptake of the nanoparticles by cells, mBMSCs were cultured with rhodamine-labeled nanoparticles for 24 h and were observed by CLSM (Figure S2). The nanoparticles, cytoskeletons, and nuclei were red, green and blue, respectively. From the merged images, both ChNC and HNT aggregates appeared inside the cells and the cells could internalize the 1D nanoparticles by endocytosis. It showed that it was feasible that both HNTs and ChNCs could be labeled with rhodamine B to track the cells, and it was promised that rhodamine-labeled nanoparticles could be used in bioimaging.

For further investigation of cytotoxicity, cell apoptosis rate (Q2 + Q4) was quantitatively determined using the annexin V−FITC/PI apoptosis detection kit. As shown in Figure 4, cell apoptosis rates of materials groups had no obvious differences with the control groups at nanoparticle concentration below 50 μg/mL. Although the ChNC group had the cell apoptosis rate

DOI: 10.1021/acssuschemeng.9b04365
ACS Sustainable Chem. Eng. 2019, 7, 18965−18975

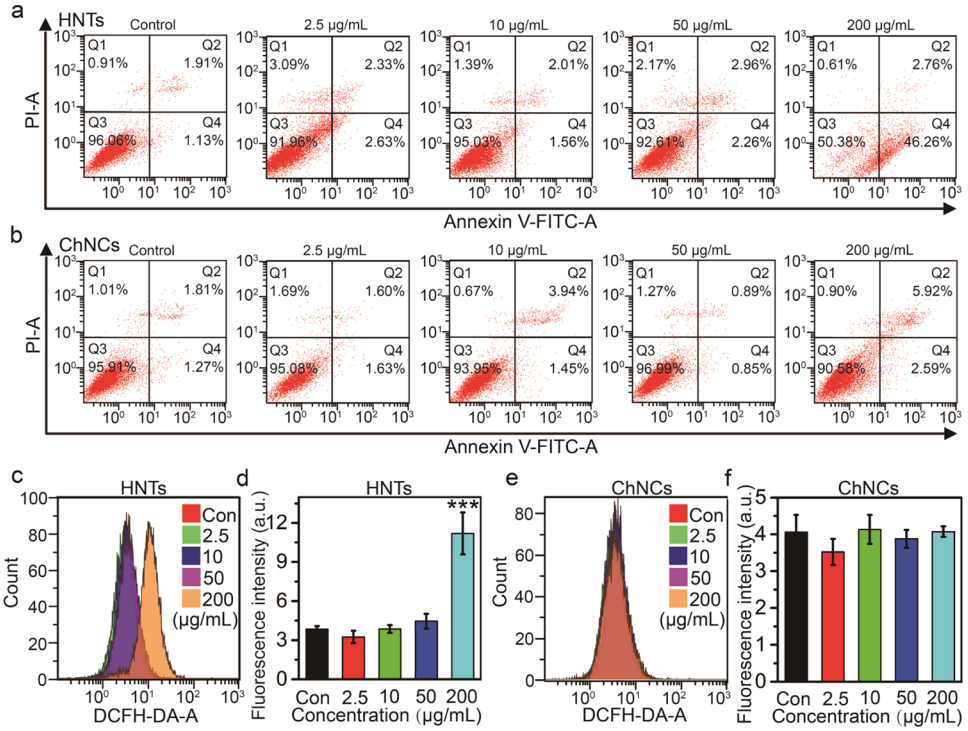

Figure 4. mBMSC apoptosis and necrosis effects of HNTs (a) and ChNCs (b), ROS production effects of HNTs (c) and ChNCs (e), and bar graph representation for ROS generation corresponding to HNTs (d) and ChNCs (f) (means ± SD, n =3).

of 8.51%, it was higher than the other groups at the concentration of 200 μg/mL. However, at the same concentration, the cell apoptosis rate of the HNT group reached to 49.02% and was significantly higher than all of the others. It was proved that ROS generation could be as a major paradigm of nanotoxicity and lead to damage of multiple cell organelles.[62,63] From Figure 4c, the mean fluorescence intensity of the 200 μg/mL HNT group shifted toward a higher value than that of the other HNT groups and greatly increased the ROS generation. In contrast, all of the ChNC groups had no obvious difference in ROS generation. These results were consisted with the previous cell LIVE/DEAD staining, viability, and apoptosis results. ChNCs presented a better biocompatibility than HNTs at the concentration of 200 μg/mL.

Distribution and Translocation of HNTs and ChNCs in Wild-Type Nematodes. To understand whether and how HNTs and ChNCs are ingested by worms, HNTs and ChNCs were labeled using rhodamine B. *C. elegans* were incubated with these rhodamine-labeled nanoparticles at L1 larvae stage for 24 or 48 h and subsequently imaged. Figure 5 shows representative nematodes with obvious red fluorescence in the intestine after exposure for either 24 or 48 h. In addition, we did not see any aggregation of the HNTs and ChNCs in the other tissues of *C. elegans* including vulva, uterus, and germline. Taken together, these results suggested that worms could eat HNTs and ChNCs through the pharynx into the intestine, as well as just uptake nanomaterials, not digesting and absorbing them.

Uptake of HNTs and ChNCs by *C. elegans* is mainly distributed in intestine, which is the main part of the nematode responsible for metabolism. Whether the location of HNTs and ChNCs in the intestine will affect the metabolism of nematodes? It was detected through lipid metabolism by oil

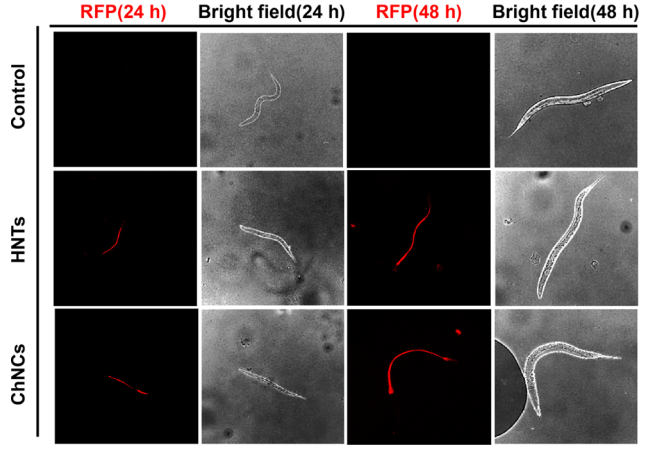

Figure 5. Translocation and distribution of HNTs and ChNCs in wild-type nematodes.

red O (ORO) staining. It was found that wild-type animals treated with different concentrations of HNTs and ChNCs did not influence ORO staining (Figure S3), which indicated that distribution of HNTs and ChNCs in the intestine did not affect its metabolic function. In addition, we further analyzed the effect of HNTs and ChNCs on the intestine function of worms by the dye leakage assay. The result showed that HNTs and ChNCs did not influence the intestinal barrier function of *C. elegans* because they had no significant effect on dye leakage of animals (Figure S4).

Toxic Effects of HNTs and ChNCs on the Reproduction and Growth of *C. elegans*. Changes in the phenotype of nematodes including body length, locomotion, and reproduction are critical endpoints in toxicology. It was analyzed the effects of body length effected by 1D nanoparticles and found that increasing concentration of HNTs and

DOI: 10.1021/acssuschemeng.9b04365
ACS Sustainable Chem. Eng. 2019, 7, 18965−18975

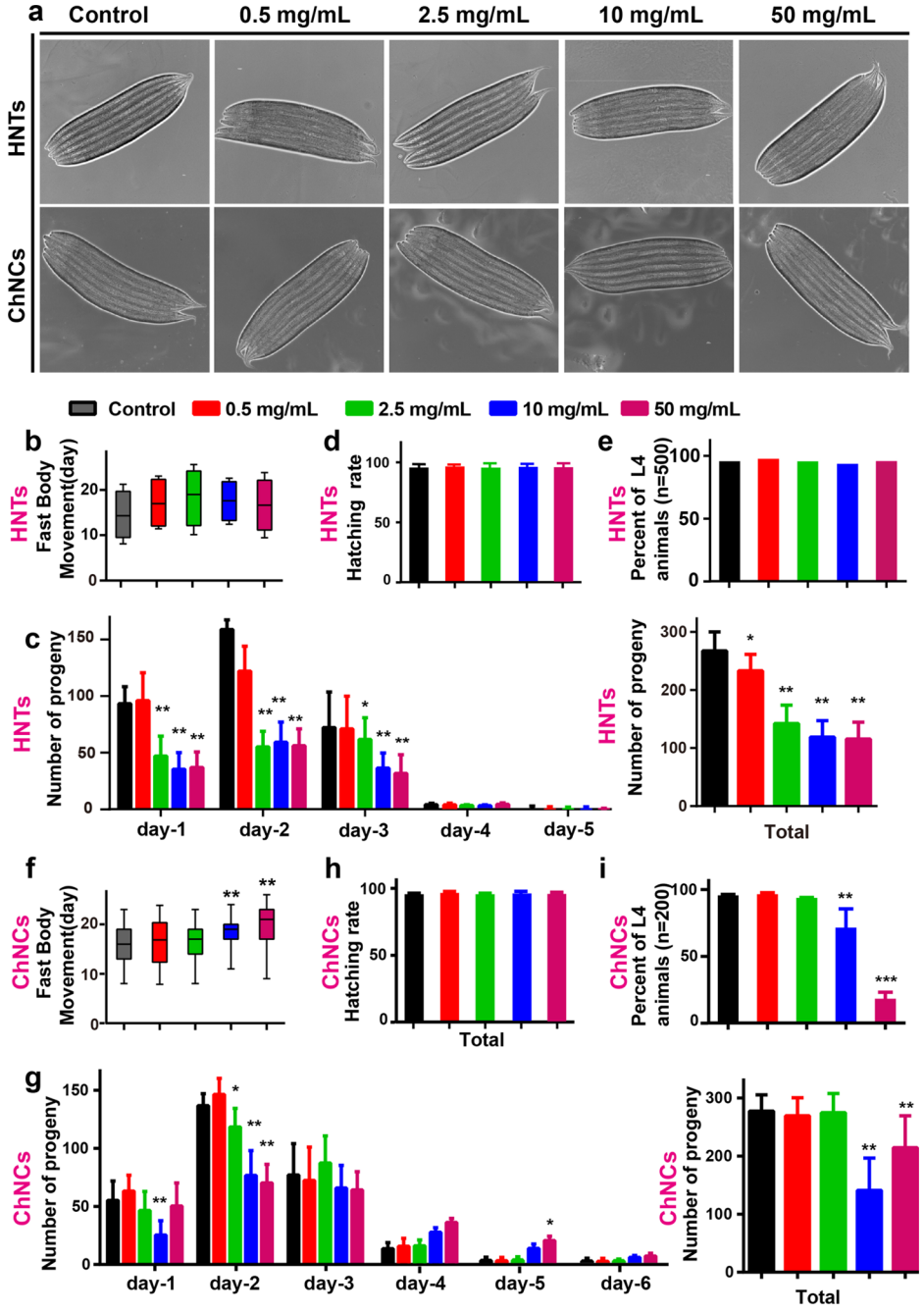

Figure 6. Effects of different HNT and ChNC concentrations on (a) worm body length, (b, f) worm locomotion ($n \geq 60$ worms for each experimental group). (c, g) Number of daily progeny and the total number of progeny of wild-type N2 worms. (d, h) Egg hatching rate of wild-type N2 worms; Student's t test; $^{*}p < 0.05$, $^{**}p < 0.01$; mean ± SD; $n \geq 30$. (e, i) Worm development ($n \geq 30$).

ChNCs did not obviously influence the body length (Figure 6a). Additionally, the body movement of animals treated with or without different concentrations of HNTs and ChNCs was analyzed. Body movement is the one of most obvious behavioral abnormalities accompanying nematode aging.[45] The results exhibited that the body movement of *C. elegans* was not influenced by HNTs (Figure 6b). However, the decrease in body movement with aging was delayed by a higher concentration of ChNCs (10 and 50 mg/mL) because the fast motion period of worms was increased, but not at other concentrations (Figure 6f). The longer fast movement periods of *C. elegans* at the higher concentrations of ChNCs could retain, which demonstrated that *C. elegans* could be in a young state at longer periods. Since worms were known to generate their progenies during the initial 5 days of adulthood, it was speculated that the early effects of materials on nematode toxicity can be reflected in the process of reproduction. Results displayed that the total brood sizes of worms were significantly decreased when animals were exposed to the different concentrations of HNTs and higher concentrations of ChNCs (10 and 50 mg/mL) (Figure 6c,g), while the hatching rate of worms was not influenced by different concentrations of HNTs or ChNCs (Figure 6d,h). Development is a critical indicator to evaluate the toxic effects of HNTs and ChNCs on larvae. Our results showed that the development of worms was not influenced by exposure to HNTs but was obviously

DOI: 10.1021/acssuschemeng.9b04365
ACS Sustainable Chem. Eng. 2019, 7, 18965−18975

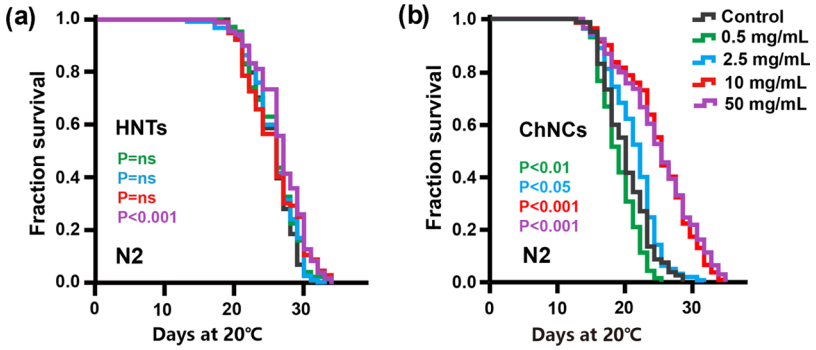

Figure 7. Effects of different concentrations of (a) HNTs and (b) ChNCs on worm lifespan. Lifespan was analyzed using the Kaplan−Meier test, and p values calculated using the log-rank test; no significance was abbreviated as ns; $n \geq 60$. Data are representative of at least two independent experiments.

decreased when animals were incubated with higher concentrations of ChNCs (10 and 50 mg/mL) (Figure 6e,i). These results demonstrated that the side effects of HNTs on *C. elegans* are relatively small, only manifested in affecting the brood size. However, ChNCs did not result in evident alterations in the phenotype of worms at lower concentrations, but at higher concentrations (10 and 50 mg/mL), their side effects are obvious, including affecting the reproduction, development, and locomotion of *C. elegans*.

Toxic Effects of HNTs and ChNCs on the Lifespan of *C. elegans*. Lifespan can reflect the long-term effect of certain toxicants on animals. Our results showed that the lifespan of *C. elegans* was hardly affected by exposure to HNTs, except animals exposed to 50 mg/mL exhibited a slight increase in the lifespan (5.4%) (Figure 7a). Different from HNTs, the lifespan of *C. elegans* was significantly influenced by ChNCs. When animals were exposed to 0.5 mg/mL ChNCs, the lifespan was moderately decreased (5.6%); however, when they were exposed to higher concentrations (2.5, 10, and 50 mg/mL), the lifespan were obviously extended (5.8, 24.4, 24.8%, respectively). This result was in agreement with the movement behavior that *C. elegans* could be in a young state at longer periods and higher concentrations of ChNCs. These variations of lifespan may be associated with the decrease in the brood size since some research works reported that a decrease in the production of progeny was usually accompanied by lifespan extension.[64,65] Therefore, only the reproduction of *C. elegans* was influenced by HNTs and other phenotypes including body length, movement ability, development, and lifespan were hardly disturbed. It indicated that HNTs had no long-term toxicological effects. Compared with HNTs, ChNCs at 10 and 50 mg/mL concentrations had effects on the reproduction and development of *C. elegans* but could retain the longer fast movement periods of *C. elegans* and promote the lifespan extension, which suggested that ChNCs not only had good biocompatibility but also could extend the lifespan. Both HNTs and ChNCs did not exhibit an obvious toxic effect, although they have particle sizes >100 nm.

Effects of HNTs and ChNCs on Induction of ROS. In *C. elegans*, oxidative stress is usually an important contributor to the toxicity induced by environmental toxicants.[66,67] It was further examined the effects of HNTs and ChNCs on inducing ROS production. It was found that HNTs and ChNCs at the different concentrations did not obviously induce the ROS production by MitoSOX staining, instead animals exposed to 50 mg/mL showed moderately decreased ROS production (Figure 8a). In addition, it was analyzed the effect of different

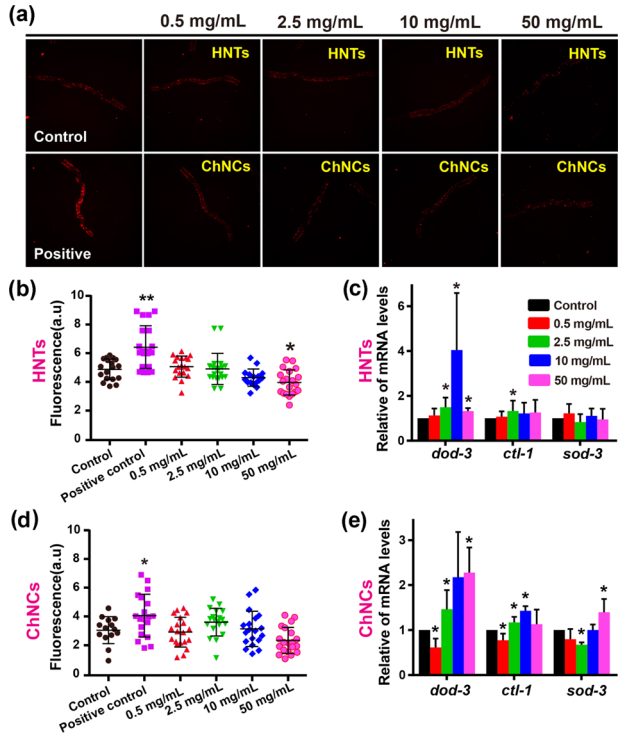

Figure 8. Effects of different concentrations of HNTs and ChNCs on ROS production. (a) Intestinal ROS production in nematode. (b, d) Fluorescence quantitation ($n \geq 30$). (c, e) qPCR analysis of the mRNA level of genes associated with the oxidative stress. Paraquat (5 mM) was used as a positive control. Data are the mean ± SD, $n = 3$, $^{*}p < 0.05$, $^{**}p < 0.01$; (Student's t test).

concentration of HNTs and ChNCs on expression levels of genes related to oxidative stress, including *dod-3*, *ctl-1*, and *sod-3*. *sod-3*, a superoxide dismutase and *ctl-1*, a catalase, serve as important molecular basis for antioxidative stress response in *C. elegans*.[68] *dod-3* as a target gene of Forkhead box O transcription factor homolog DAF-16 is closely associated with the oxidative stress.[69]

Our results displayed that expression of these oxidative stress-associated genes was hardly affected by HNTs, just *dod-3* level was slightly elevated when animals exposed to concentrations of 2.5, 10, and 50 mg/mL and *ctl-1* level was increased when worms were exposed to a concentration of 10 mg/mL. However, for ChNCs, the expression of *dod-3*, *ctl-1*, and *sod-3* was downregulated at low concentrations (0.5 mg/

DOI: 10.1021/acssuschemeng.9b04365
ACS Sustainable Chem. Eng. 2019, 7, 18965−18975

mL), but the expression of these genes was upregulated at high concentrations (2.5, 10, and 50 mg/mL). This result of expression was consistent with lifespan analysis; when animals were exposed to 0.5 mg/mL, the shortening of lifespan might be related to the downregulation of the expression of *dod-3*, *ctl-1*, and *sod-3*, while at high concentrations (2.5, 10, and 50 mg/mL), ChNCs induced a slight oxidative stress, which in turn upregulated oxidative stress-related genes, ultimately leading to extending lifespan. These results suggested that when the nematodes were treated with HNTs and ChNCs, a slight oxidative stress might be induced, which in turn leads to a slight upregulation of the oxidation-related genes and ultimately does not cause a significant increase in ROS production.

CONCLUSIONS

Here, toxicity of two 1D nanoparticles was systematically discussed. In vitro, mBMSCs and UMR-106 were used to evaluate the toxicity. Cell staining results showed that there were massive dead cells including mBMSCs and UMR-106 at the HNT concentration of 200 μg/mL. Cell viabilities of mBMSCs and UMR-106 were 73.4 and 77.1%, respectively, at a concentration of 200 μg/mL. LIVE/DEAD staining and cell viability at low dose groups showed that HNTs and ChNCs had no obvious difference. Cell apoptosis and ROS generation results agree with LIVE/DEAD staining and cell viability. It proved that HNTs at the concentration of 200 μg/mL had the obvious cytotoxicity. CLSM images demonstrated that rhodamine-labeled nanoparticles could enter into mBMSCs. In vivo, the results of the *C. elegans* model showed that HNTs and ChNCs were distributed in the intestine of *C. elegans* and did not affect the metabolic function of the intestine. The body length was hardly influenced by the 1D nanoparticles. HNTs had an effect on the reproduction of *C. elegans* but not on the other phenotypes including movement ability, development, and lifespan. Thus, HNTs had not a long-term toxicity. In contrast, there were no obvious effects on phenotypes below the 2.5 mg/mL concentration of ChNCs. Reproduction and development of *C. elegans* were influenced negatively on being exposed to ChNCs at the concentrations of 10 and 50 mg/mL but could retain the longer fast movement periods and extend the lifespan of *C. elegans*. It demonstrated that ChNCs had good biocompatibility and could prolong the life of *C. elegans*. Finally, the oxidative stress was investigated to study the toxicological mechanism of nanoparticles from a molecular level. The results showed that *C. elegans* were treated with HNTs and ChNCs to induce a slight oxidative stress. It leads to a slight upregulation of the oxidation-related genes but did not cause a significant increase in ROS production. The *C. elegans* experiments suggested that both ChNCs and HNTs below the concentration of 50 mg/mL had no obvious toxicity, so the nanoparticles showed promising applications in biomedical areas.

ASSOCIATED CONTENT

Supporting Information

The Supporting Information is available free of charge on the ACS Publications website at DOI: 10.1021/acssuschemeng.9b04365.

Appearance of HNT and ChNC suspensions after standing for 3 days; CLSM images of mBMSCs cocultured with rhodamine-labeled HNTs and ChNCs; effects of HNTs and ChNCs on lipid metabolism of *C. elegans*; and dye leakage assay of wild-type animals treated with HNTs and ChNCs (PDF)

AUTHOR INFORMATION

Corresponding Authors

*E-mail: gene@email.jnu.edu.cn (Q.Z.).
*E-mail: liumx@jnu.edu.cn (M.L.).

ORCID

Qinghua Zhou: 0000-0003-0468-9266
Mingxian Liu: 0000-0002-5466-3024

Author Contributions

‖X.Z. and Q.W. contributed equally to this work.

Notes

The authors declare no competing financial interest.

ACKNOWLEDGMENTS

This work was financially supported by the National Natural Science Foundation of China (51502113 and 81601299), the Program of Introducing Talents of Discipline to Universities (111 Project, No. B16021), China Postdoctoral Science Special Fund (2018M633288), Guangdong Basic and Applied Basic Research Foundation (2019A1515011509), and the Fundamental Research Funds for the Central Universities (21619102).

REFERENCES

(1) Valsami-Jones, E.; Lynch, I. How Safe are Nanomaterials? *Science* **2015**, *350*, 388−389.
(2) Blanco, E.; Shen, H.; Ferrari, M. Principles of Nanoparticle Design for Overcoming Biological Barriers to Drug Delivery. *Nat. Biotechnol.* **2015**, *33*, 941−951.
(3) Nel, A.; Xia, T.; Mädler, L.; Li, N. Toxic Potential of Materials at the Nanolevel. *Science* **2006**, *311*, 622−627.
(4) Kostarelos, K.; Lacerda, L.; Pastorin, G.; Wu, W.; Wieckowski, S.; Luangsivilay, J.; Godefroy, S.; Pantarotto, D.; Briand, J.-P.; Muller, S.; et al. Cellular Uptake of Functionalized Carbon Nanotubes is Independent of Functional Group and Cell Type. *Nat. Nanotechnol.* **2007**, *2*, 108−113.
(5) Chithrani, B. D.; Ghazani, A. A.; Chan, W. C. W. Determining the Size and Shape Dependence of Gold Nanoparticle Uptake into Mammalian Cells. *Nano Lett.* **2006**, *6*, 662−668.
(6) Joussein, E.; Petit, S.; Churchman, J.; Theng, B.; Righi, D.; Delvaux, B. Halloysite Clay Minerals -a Review. *Clay Miner.* **2005**, *40*, 383−426.
(7) Tully, J.; Yendluri, R.; Lvov, Y. Halloysite Clay Nanotubes for Enzyme Immobilization. *Biomacromolecules* **2016**, *17*, 615−621.
(8) Liu, M.; Jia, Z.; Jia, D.; Zhou, C. Recent Advance in Research on Halloysite Nanotubes-Polymer Nanocomposite. *Prog. Polym. Sci.* **2014**, *39*, 1498−1525.
(9) Zhao, N.; Liu, Y.; Zhao, X.; Song, H. Liquid Crystal Self-assembly of Halloysite Nanotubes in Ionic Liquids: a Novel Soft Nanocomposite Ionogel Electrolyte with High Anisotropic Ionic conductivity and thermal stability. *Nanoscale* **2016**, *8*, 1545−1554.
(10) Chen, L.; Jia, Z.; Guo, X.; Zhong, B.; Chen, Y.; Luo, Y.; Jia, D. Functionalized HNTs Nanocluster Vulcanized Natural Rubber with High Filler-Rubber Interaction. *Chem. Eng. J.* **2018**, *336*, 748−756.
(11) Lin, Y.; Wang, X.; Liu, J.; Miller, J. D. Natural Halloysite Nano-clay Electrolyte for Advanced all-Solid-State Lithium-Sulfur Batteries. *Nano Energy* **2017**, *31*, 478−485.
(12) Massaro, M.; Cavallaro, G.; Colletti, C. G.; Lazzara, G.; Milioto, S.; Noto, R.; Riela, S. Chemical Modification of Halloysite Nanotubes for Controlled Loading and Release. *J. Mater. Chem. B* **2018**, *6*, 3415−3433.

DOI: 10.1021/acssuschemeng.9b04365
ACS Sustainable Chem. Eng. 2019, 7, 18965−18975

(13) Liu, M.; Fakhrullin, R.; Novikov, A.; Panchal, A.; Lvov, Y. Tubule Nanoclay-Organic Heterostructures for Biomedical Applications. *Macromol. Biosci.* **2019**, *19*, No. 1800419.
(14) Massaro, M.; Buscemi, G.; Arista, L.; Biddeci, G.; Cavallaro, G.; D'Anna, F.; Di Blasi, F.; Ferrante, A.; Lazzara, G.; Rizzo, C.; Spinelli, G.; Ullrich, T.; Riela, S. Multifunctional Carrier Based on Halloysite/Laponite Hybrid Hydrogel for Kartogenin Delivery. *ACS Med. Chem. Lett.* **2019**, *10*, 419−424.
(15) Massaro, M.; Lazzara, G.; Milioto, S.; Noto, R.; Riela, S. Covalently Modified Halloysite Clay Nanotubes: Synthesis, Properties, Biological and Medical Applications. *J. Mater. Chem. B* **2017**, *5*, 2867−2882.
(16) Massaro, M.; Colletti, C. G.; Guernelli, S.; Lazzara, G.; Liu, M.; Nicotra, G.; Noto, R.; Parisi, F.; Pibiri, I.; Spinella, C.; Riela, S. Photoluminescent Hybrid Nanomaterials from Modified Halloysite Nanotubes. *J. Mater. Chem. C* **2018**, *6*, 7377−7384.
(17) Massaro, M.; Barone, G.; Biddeci, G.; Cavallaro, G.; Di Blasi, F.; Lazzara, G.; Nicotra, G.; Spinella, C.; Spinelli, G.; Riela, S. Halloysite Nanotubes-Carbon Dots Hybrids Multifunctional Nanocarrier with Positive Cell Target Ability as a Potential Non-Viral Vector for Oral Gene Therapy. *J. Colloid Interface Sci.* **2019**, *552*, 236−246.
(18) Fakhrullina, G. I.; Akhatova, F. S.; Lvov, Y. M.; Fakhrullin, R. F. Toxicity of Halloysite Clay Nanotubes in Vivo: a *Caenorhabditis elegans* Study. *Environ. Sci. Nano* **2015**, *2*, 54−59.
(19) Long, Z.; Wu, Y.-P.; Gao, H.-Y.; Zhang, J.; Ou, X.; He, R.-R.; Liu, M. In Vitro and in Vivo Toxicity Evaluation of Halloysite Nanotubes. *J. Mater. Chem. B* **2018**, *6*, 7204−7216.
(20) Wang, X.; Gong, J.; Rong, R.; Gui, Z.; Hu, T.; Xu, X. Halloysite Nanotubes-Induced Al Accumulation and Fibrotic Response in Lung of Mice after 30-Day Repeated Oral Administration. *J. Agric. Food. Chem.* **2018**, *66*, 2925−2933.
(21) Vergaro, V.; Abdullayev, E.; Lvov, Y. M.; Zeitoun, A.; Cingolani, R.; Rinaldi, R.; Leporatti, S. Cytocompatibility and Uptake of Halloysite Clay Nanotubes. *Biomacromolecules* **2010**, *11*, 820−826.
(22) Dzamukova, M. R.; Naumenko, E. A.; Lvov, Y. M.; Fakhrullin, R. F. Enzyme-Activated Intracellular Drug Delivery with Tubule Clay Nanoformulation. *Sci. Rep.* **2015**, *5*, No. 10560.
(23) Bellani, L.; Giorgetti, L.; Riela, S.; Lazzara, G.; Scialabba, A.; Massaro, M. Ecotoxicity of Halloysite Nanotube-Supported Palladium Nanoparticles in *Raphanus sativus* L. *Environ. Toxicol. Chem.* **2016**, *35*, 2503−2510.
(24) Rinaudo, M. Chitin and Chitosan: Properties and Applications. *Prog. Polym. Sci.* **2006**, *31*, 603−632.
(25) Duan, B.; Zheng, X.; Xia, Z.; Fan, X.; Guo, L.; Liu, J.; Wang, Y.; Ye, Q.; Zhang, L. Highly Biocompatible Nanofibrous Microspheres Self-Assembled from Chitin in NaOH/Urea Aqueous Solution as Cell Carriers. *Angew. Chem., Int. Ed.* **2015**, *54*, 5152−5156.
(26) Lin, N.; Huang, J.; Dufresne, A. Preparation, Properties and Applications of Polysaccharide Nanocrystals in Advanced Functional Nanomaterials: a Review. *Nanoscale* **2012**, *4*, 3274−3294.
(27) Gopalan Nair, K.; Dufresne, A. Crab Shell Chitin Whisker Reinforced Natural Rubber Nanocomposites. 1. Processing and Swelling Behavior. *Biomacromolecules* **2003**, *4*, 657−665.
(28) Huang, Y.; Yao, M.; Zheng, X.; Liang, X.; Su, X.; Zhang, Y.; Lu, A.; Zhang, L. Effects of Chitin Whiskers on Physical Properties and Osteoblast Culture of Alginate Based Nanocomposite Hydrogels. *Biomacromolecules* **2015**, *16*, 3499−3507.
(29) Liu, Y.; Liu, M.; Yang, S.; Luo, B.; Zhou, C. Liquid Crystalline Behaviors of Chitin Nanocrystals and Their Reinforcing Effect on Natural Rubber. *ACS Sustainable Chem. Eng.* **2018**, *6*, 325−336.
(30) Tran, T. H.; Nguyen, H.-L.; Hwang, D. S.; Lee, J. Y.; Cha, H. G.; Koo, J. M.; Hwang, S. Y.; Park, J.; Oh, D. X. Five Different Chitin Nanomaterials from Identical Source with Different Advantageous Functions and Performances. *Carbohydr. Polym.* **2019**, *205*, 392−400.
(31) Qiu, T. A.; Clement, P. L.; Haynes, C. L. Linking Nanomaterial Properties to Biological Outcomes: Analytical Chemistry Challenges in Nanotoxicology for the Next Decade. *Chem. Commun.* **2018**, *54*, 12787−12803.
(32) Villanueva, M. E.; Salinas, A.; Díaz, L. E.; Copello, G. J. Chitin Nanowhiskers as Alternative Antimicrobial Controlled Release Carriers. *New J. Chem.* **2015**, *39*, 614−620.
(33) Ou, X.; Zheng, J.; Zhao, X.; Liu, M. Chemically Cross-Linked Chitin Nanocrystal Scaffolds for Drug Delivery. *ACS Appl. Nano Mater.* **2018**, *1*, 6790−6799.
(34) Wu, Q.; Li, Y.; Li, Y.; Zhao, Y.; Ge, L.; Wang, H.; Wang, D. Crucial Role of the Biological Barrier at the Primary Targeted Organs in Controlling the Translocation and Toxicity of Multi-walled Carbon Nanotubes in the Nematode *Caenorhabditis elegans*. *Nanoscale* **2013**, *5*, 11166−11178.
(35) Gonzalez-Moragas, L.; Maurer, L. L.; Harms, V. M.; Meyer, J. N.; Laromaine, A.; Roig, A. Materials and Toxicological Approaches to Study Metal and Metal-oxide Nanoparticles in the Model Organism *Caenorhabditis elegans*. *Mater. Horiz.* **2017**, *4*, 719−746.
(36) Zhi, L.; Qu, M.; Ren, M.; Zhao, L.; Li, Y.; Wang, D. Graphene Oxide Induces Canonical Wnt/β-catenin Signaling-Dependent Toxicity in *Caenorhabditis elegans*. *Carbon* **2017**, *113*, 122−131.
(37) Zhao, Y.; Wang, X.; Wu, Q.; Li, Y.; Wang, D. Translocation and Neurotoxicity of CdTe Quantum Dots in RMEs Motor Neurons in Nematode *Caenorhabditis elegans*. *J. Hazard. Mater.* **2015**, *283*, 480−489.
(38) Däwlätşina, G. I.; Minullina, R. T.; Fakhrullin, R. F. Microworms Swallow the Nanobait: the Use of Nanocoated Microbial Cells for the Direct Delivery of Nanoparticles into *Caenorhabditis elegans*. *Nanoscale* **2013**, *5*, 11761−11769.
(39) Tryfon, P.; Antonoglou, O.; Vourlias, G.; Mourdikoudis, S.; Menkisoglou, O.; Dendrinou-Samara, C. Tailoring Ca-Based Nanoparticles by Polyol Process for Use as Nematicidals and pH Adjusters in Agriculture. *ACS Appl. Nano Mater.* **2019**, *2*, 3870−3881.
(40) Konnova, S.; Danilushkina, A.; Fakhrullina, G.; Akhatova, F.; Badrutdinov, A.; Fakhrullin, R. Silver Nanoparticle-Coated "cyborg" Microorganisms: Rapid Assembly of Polymer-Stabilised Nanoparticles on Microbial Cells. *RSC Adv.* **2015**, *5*, 13530−13537.
(41) Fakhrullina, G.; Khakimova, E.; Akhatova, F.; Lazzara, G.; Parisi, F.; Fakhrullin, R. Selective Antimicrobial Effects of Curcumin@Halloysite Nanoformulation: A *Caenorhabditis elegans* Study. *ACS Appl. Mater. Interfaces* **2019**, *11*, 23050−23064.
(42) Richter, K.; Facal, P.; Thomas, N.; Vandecandelaere, I.; Ramezanpour, M.; Cooksley, C.; Prestidge, C. A.; Coenye, T.; Wormald, P.-J.; Vreugde, S. Taking the Silver Bullet Colloidal Silver Particles for the Topical Treatment of Biofilm-Related Infections. *ACS Appl. Mater. Interfaces* **2017**, *9*, 21631−21638.
(43) Zeng, J.-B.; He, Y.-S.; Li, S.-L.; Wang, Y.-Z. Chitin Whiskers: an Overview. *Biomacromolecules* **2012**, *13*, 1−11.
(44) Wan, Q. L.; Zheng, S. Q.; Wu, G. S.; Luo, H. R. Aspirin Extends the Lifespan of *Caenorhabditis elegans* via AMPK and DAF-16/FOXO in Dietary Restriction Pathway. *Exp. Gerontol.* **2013**, *48*, 499−506.
(45) Huang, C.; Xiong, C.; Kornfeld, K. Measurements of Age-Related Changes of Physiological Processes that Predict Lifespan of *Caenorhabditis elegans*. *Proc. Natl. Acad. Sci. U.S.A.* **2004**, *101*, 8084−8089.
(46) Brenner, S. The genetics of *Caenorhabditis elegans*. *Genetics* **1974**, *77*, 71−94.
(47) Zhou, Q.; Li, H.; Li, H.; Nakagawa, A.; Lin, J. L.; Lee, E.-S.; Harry, B. L.; Skeen-Gaar, R. R.; Suehiro, Y.; William, D.; et al. Mitochondrial Endonuclease G Mediates Breakdown of Paternal Mitochondria upon Fertilization. *Science* **2016**, *353*, 394−399.
(48) Ryu, D.; Mouchiroud, L.; Andreux, P. A.; Katsyuba, E.; Moullan, N.; Nicolet-dit-Félix, A. A.; Williams, E. G.; Jha, P.; Lo Sasso, G.; Huzard, D.; Aebischer, P.; Sandi, C.; Rinsch, C.; Auwerx, J. Urolithin A Induces Mitophagy and Prolongs Lifespan in *C. elegans* and Increases Muscle Function in Rodents. *Nat. Med.* **2016**, *22*, 879−888.
(49) O'Rourke, E. J.; Soukas, A. A.; Carr, C. E.; Ruvkun, G. *C. elegans* Major Fats are Stored in Vesicles Distinct From Lysosome-Related Organelles. *Cell Metab.* **2009**, *10*, 430−435.

DOI: 10.1021/acssuschemeng.9b04365
ACS Sustainable Chem. Eng. 2019, 7, 18965−18975

(50) Hoogewijs, D.; Houthoofd, K.; Matthijssens, F.; Vandesompele, J.; Vanfleteren, J. R. Selection and Validation of a Set of Reliable Reference Genes for Quantitative Sod Gene Expression Analysis in *C. elegans*. *BMC Mol. Biol.* **2008**, *9*, No. 9.
(51) Gelino, S.; Chang, J. T.; Kumsta, C.; She, X.; Davis, A.; Nguyen, C.; Panowski, S.; Hansen, M. Intestinal Autophagy Improves Healthspan and Longevity in *C. elegans* During Dietary Restriction. *PLoS Genet.* **2016**, *12*, No. e1006135.
(52) Choi, S.-J.; Choy, J.-H. Effect of Physico-Chemical Parameters on the Toxicity of Inorganic Nanoparticles. *J. Mater. Chem.* **2011**, *21*, 5547−5554.
(53) Chen, M.; Li, Y.; Zhou, J.; Yang, Z.; Wang, Z.; Yang, Y.; Zhang, H.; Li, Z.; Mei, X. In Vitro Toxicity Assessment of Nanocrystals in Tissue-Type Cells and Macrophage Cells. *J. Appl. Toxicol.* **2018**, *38*, 656−664.
(54) Xi, W.-S.; Song, Z.-M.; Chen, Z.; Chen, N.; Yan, G.-H.; Gao, Y.; Cao, A.; Liu, Y.; Wang, H. Short-term and Long-term Toxicological Effects of Vanadium Dioxide Nanoparticles on A549 Cells. *Environ. Sci. Nano* **2019**, *6*, 565−579.
(55) Puisney, C.; Oikonomou, E. K.; Nowak, S.; Chevillot, A.; Casale, S.; Baeza-Squiban, A.; Berret, J.-F. Brake Wear (nano) Particle Characterization and Toxicity on Airway Epithelial Cells in Vitro. *Environ. Sci. Nano* **2018**, *5*, 1036−1044.
(56) Anders, C. B.; Eixenberger, J. E.; Franco, N. A.; Hermann, R. J.; Rainey, K. D.; Chess, J. J.; Punnoose, A.; Wingett, D. G. ZnO Nanoparticle Preparation Route Influences Surface Reactivity, Dissolution and Cytotoxicity. *Environ. Sci. Nano* **2018**, *5*, 572−588.
(57) Joris, F.; Valdepérez, D.; Pelaz, B.; Wang, T.; Doak, S. H.; Manshian, B. B.; Soenen, S. J.; Parak, W. J.; De Smedt, S. C.; Raemdonck, K. Choose your Cell Model Wisely: The in Vitro Nanoneurotoxicity of Differentially Coated Iron Oxide Nanoparticles for Neural Cell Labeling. *Acta Biomater.* **2017**, *55*, 204−213.
(58) Joris, F.; Valdepérez, D.; Pelaz, B.; Soenen, S. J.; Manshian, B. B.; Parak, W. J.; De Smedt, S. C.; Raemdonck, K. The Impact of Species and Cell Type on the Nanosafety Profile of Iron Oxide Nanoparticles in Neural Cells. *J. Nanobiotechnol.* **2016**, *14*, No. 69.
(59) Chen, F.; Li, G.; Zhao, E. R.; Li, J.; Hableel, G.; Lemaster, J. E.; Bai, Y.; Sen, G. L.; Jokerst, J. V. Cellular Toxicity of Silicon Carbide Nanomaterials as a Function of Morphology. *Biomaterials* **2018**, *179*, 60−70.
(60) Yang, J.; Wu, Y.; Shen, Y.; Zhou, C.; Li, Y.-F.; He, R.-R.; Liu, M. Enhanced Therapeutic Efficacy of Doxorubicin for Breast Cancer Using Chitosan Oligosaccharide-Modified Halloysite Nanotubes. *ACS Appl. Mater. Interfaces* **2016**, *8*, 26578−26590.
(61) Pillai, C. K. S.; Paul, W.; Sharma, C. P. Chitin and Chitosan Polymers: Chemistry, Solubility and Fiber Formation. *Prog. Polym. Sci.* **2009**, *34*, 641−678.
(62) Wang, Y.; Kaur, G.; Zysk, A.; Liapis, V.; Hay, S.; Santos, A.; Losic, D.; Evdokiou, A. Systematic in Vitro Nanotoxicity Study on Anodic Alumina Nanotubes with Engineered Aspect Ratio: Understanding Nanotoxicity by a Nanomaterial Model. *Biomaterials* **2015**, *46*, 117−130.
(63) Gollavelli, G.; Ling, Y.-C. Multi-Functional Graphene as an in Vitro and in Vivo Imaging Probe. *Biomaterials* **2012**, *33*, 2532−2545.
(64) Hsin, H.; Kenyon, C. Signals from the Reproductive System Regulate the Lifespan of *C. elegans*. *Nature* **1999**, *399*, 362−366.
(65) Herndon, L. A.; Wolkow, C. A.; Driscoll, M.; Hall, D. H. Effects of Ageing on the Basic Biology and Anatomy of *C. elegans*. In *Ageing: Lessons from C. elegans*; Olsen, A., Gill, M., Eds.; Springer: Cham, 2017; pp 9−39.
(66) Ren, M.; Zhao, L.; Lv, X.; Wang, D. Antimicrobial Proteins in the Response to Graphene oxide in *Caenorhabditis elegans*. *Nanotoxicology* **2017**, *11*, 578−590.
(67) Hu, C.-C.; Wu, G.-H.; Hua, T.-E.; Wagner, O. I.; Yen, T.-J. Uptake of TiO_2 Nanoparticles into *C. elegans* Neurons Negatively Affects Axonal Growth and Worm Locomotion Behavior. *ACS Appl. Mater. Interfaces* **2018**, *10*, 8485−8495.
(68) Dues, D. J.; Schaar, C. E.; Johnson, B. K.; Bowman, M. J.; Winn, M. E.; Senchuk, M. M.; Van Raamsdonk, J. M. Uncoupling of Oxidative Stress Resistance and Lifespan in Long-lived isp-1 Mitochondrial Mutants in *Caenorhabditis elegans*. *Free Radical Biol. Med.* **2017**, *108*, 362−373.
(69) Chen, A. T. Y.; Guo, C.; Dumas, K. J.; Ashrafi, K.; Hu, P. J. Effects of *Caenorhabditis elegans* sgk-1 Mutations on Lifespan, Stress resistance, and DAF-16/FoxO Regulation. *Aging Cell* **2013**, *12*, 932−940.

DOI: 10.1021/acssuschemeng.9b04365
ACS Sustainable Chem. Eng. 2019, 7, 18965−18975